Analytical Biochemistry 465 (2014) 105–113

Contents lists available at ScienceDirect

Analytical Biochemistry

journal homepage: www.elsevier.com/locate/yabio

High-performance liquid chromatography-based method to evaluate kinetics of glucosinolate hydrolysis by *Sinapis alba* myrosinase

Kayla J. Vastenhout, Ruthellen H. Tornberg, Amanda L. Johnson, Michael W. Amolins, Jared R. Mays *

Department of Chemistry, Augustana College, Sioux Falls, SD 57197, USA

ARTICLE INFO

Article history:
Received 19 June 2014
Accepted 15 July 2014
Available online 25 July 2014

Keywords:
Glucosinolate
Isothiocyanate
Myrosinase
Michaelis–Menten
Progress curve
HPLC

ABSTRACT

Isothiocyanates (ITCs) are one of several hydrolysis products of glucosinolates, plant secondary metabolites that are substrates for the thioglucohydrolase myrosinase. Recent pursuits toward the development of synthetic non-natural ITCs have consequently led to an exploration of generating these compounds from non-natural glucosinolate precursors. Evaluation of the myrosinase-dependent conversion of select non-natural glucosinolates to non-natural ITCs cannot be accomplished using established ultraviolet–visible (UV–Vis) spectroscopic methods. To overcome this limitation, an alternative high-performance liquid chromatography (HPLC)-based analytical approach was developed where initial reaction velocities were generated from nonlinear reaction progress curves. Validation of this HPLC method was accomplished through parallel evaluation of three glucosinolates with UV–Vis methodology. The results of this study demonstrate that kinetic data are consistent between both analytical methods and that the tested glucosinolates respond similarly to both Michaelis–Menten and specific activity analyses. Consequently, this work resulted in the complete kinetic characterization of three glucosinolates with *Sinapis alba* myrosinase, with results that were consistent with previous reports.

Organic isothiocyanates (ITCs,[1] **3**, Scheme 1) are a particularly well-studied class of compounds that demonstrate several modes of bioactivity relevant to improved human health. Many of the *Brassica* vegetables—including broccoli, spinach, cabbage, cauliflower, Brussels sprouts, kale, collard greens, pak choi, and kohlrabi—are rich sources of ITCs with documented antioxidant [1–3], anti-inflammatory [4–7], antibacterial [8–11], antifungal [12,13], and antitumor [14–17] properties. The phytochemical origin of ITCs is dietary glucosinolates (**1**), β-thioglucoside-*N*-hydroxysulfates biosynthesized by plants from amino acids. More than 200 naturally occurring glucosinolates have been identified, most of which are substrates of the enzyme myrosinase (β-thioglucoside glucohydrolase, EC 3.2.3.1), which is present in *Brassica* plants and whose mechanism follows Michaelis–Menten kinetics [18]. Myrosinase catalyzes the hydrolysis of the thioglucosidic linkage, evolving a molecule of D-glucose and an unstable intermediate (**2**) that rapidly rearranges to a variety of other organic functional groups [19]. At physiological pH and temperature, **2** predominantly undergoes a Lossen rearrangement to form an ITC (**3**) [19–21].

To maintain a consistent definition with non-natural ITCs, and to differentiate between synthetic analogues of natural glucosinolates [22–24], a non-natural glucosinolate was defined as a β-thioglucoside-*N*-hydroxysulfate containing a side chain (R, Scheme 1) not present in nature. Although select synthetic non-natural ITCs have been shown to elicit improved activity profiles versus their naturally occurring derivatives [25,26], few studies have described the ability of non-natural glucosinolates to serve as precursors for these non-natural ITCs. Investigators in a 2008 study hypothesized that myrosinase would be tolerant to the structural changes of non-natural glucosinolates and would retain its ability to hydrolyze their thioglucosidic linkages [26]. This hypothesis was supported by results demonstrating that *Sinapis alba* myrosinase catalyzed the hydrolysis of two non-natural glucosinolates, resulting in evolution of their corresponding non-natural ITCs. More recently, a 2014 study described the hydrolysis kinetics of five non-natural glucosinolates by *S. alba* myrosinase [27].

Analysis of the myrosinase-catalyzed conversion of glucosinolates to ITCs traditionally has been conducted via ultraviolet–visible (UV–Vis) spectroscopy [28]. This method has been sufficient for most natural glucosinolate/ITC pairs, whose absorbance scales

* Corresponding author. Fax: +1 605 274 4492.
E-mail address: jmays@augie.edu (J.R. Mays).

[1] *Abbreviations used:* ITC, isothiocyanate; UV–Vis, ultraviolet–visible; CE, capillary electrophoresis; HPLC, high-performance liquid chromatography; NMR, nuclear magnetic resonance; TFA, trifluoroacetic acid.

http://dx.doi.org/10.1016/j.ab.2014.07.017
0003-2697/

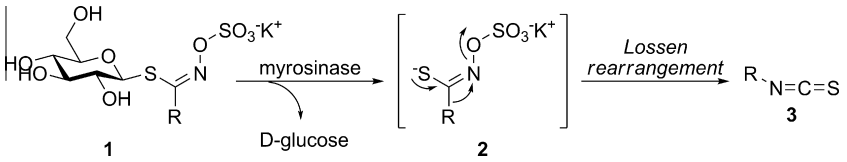

Scheme 1. Enzymatic conversion of glucosinolates to isothiocyanates by myrosinase.

linearly with aqueous concentration. A recent study by Nehmé and coworkers described a novel method to assess myrosinase kinetics using capillary electrophoresis (CE) [27]. In this approach, partially (<10%) completed reactions were electrophoretically separated and analyzed for the presence of sulfate ion, the inorganic product from the Lossen rearrangement of **2**. Although the CE method provides robust data and offers the advantages of decreased reaction volume, reduced enzyme use, and rapid (~10 min) data acquisition for a single reaction timepoint, it is dependent on sulfate ion production, an indirect measure of hydrolysis. Consequently, for studies seeking to simultaneously, directly, and differentially analyze glucosinolate, ITC, and other possible hydrolysis products (e.g., nitriles, thiocyanates), the scope of the CE approach may be limited in preference of a method that directly detects each analyte of interest [29].

Unfortunately, neither of the reported approaches accommodates the evaluation of glucosinolate/ITC pairs with limited aqueous solubility, such as the non-natural ITCs evaluated by Mays [29]. In that report, both ITCs demonstrated poor aqueous solubility, precluding analysis of their evolution from non-natural glucosinolates using UV–Vis spectroscopy. To circumvent this unforseen incompatibility, an alternative high-performance liquid chromatography (HPLC)-based method was employed where all components in a myrosinase-catalyzed hydrolysis reaction were solubilized with CH_3CN, chromatographically separated, and quantified using HPLC [26]. There are many examples describing the use of HPLC to assess reaction kinetics [30,31]. These approaches provide discontinuous data, sampled at regular intervals, from which analyte concentrations can be determined over time. Although authors rarely elaborate on the details of how initial reaction velocities (V_0 values) are obtained, it appears that most accounts generate velocities from linear regression of concentration versus time data, commonly known as a reaction progress curve. Often, restraints are placed on the total percent progress of the reaction to maintain saturation kinetics and linearity of the reaction progress curve [27].

Although the 2008 HPLC approach demonstrated the proof-of-principle enzymatic conversion of non-natural glucosinolates to non-natural ITCs, there were several aspects that devalue its general utility [26]. Foremost, the solvent gradient and reequilibration method were never optimized for rapid evaluation; each injection required 1.5 h, and each reaction was conducted over 9 h. Over this timeframe, significant ITC degradation was observed, limiting the kinetic information that could be gained concerning the formation of product. Consequently, the lengthy method, coupled with the necessity to conduct replicate trials, led to analysis of only a single initial concentration of substrate (glucosinolate) and enzyme (myrosinase); the effects of variable substrate/enzyme concentration were not evaluated, precluding formal Michaelis–Menten and specific activity analyses. Furthermore, all glucosinolates were monitored at a single wavelength (227 nm); ideally, the use of a diode array detector capable of simultaneously tracking several discrete wavelengths should provide the opportunity to validate kinetic data through standardization and analysis of several wavelengths in parallel. Lastly, and most critically, V_0 values were estimated from linear regression of nonlinear reaction progress curves

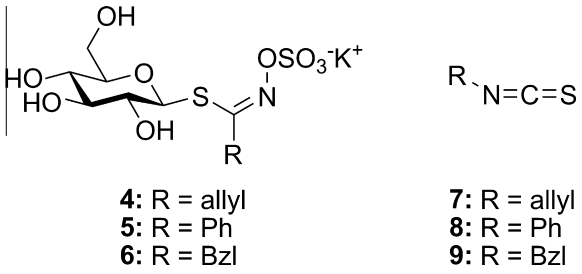

Fig.1. Target glucosinolates and isothiocyanates.

without fitting an appropriate curve generated via nonlinear regression [32–35]. Given these limitations, optimization and validation of the HPLC method would be required to strengthen its general ability to analyze the hydrolysis kinetics of non-natural glucosinolates that are not amenable to other methods.

The central hypothesis of this work was that an efficient HPLC assay could be developed to analyze myrosinase kinetics through direct and concurrent detection of both non-natural glucosinolates and non-natural ITCs. Unlike many similar approaches, this method would generate V_0 values from nonlinear reaction progress curves, increasing its ability to analyze reactions beyond early timepoints (>10% completion) or at sub-saturating conditions. Validation of this HPLC approach would be completed through parallel analysis using the established UV–Vis spectroscopy protocol, a feature that would facilitate the direct comparison of kinetic data across glucosinolate analogues and the methodologies used to analyze them.

To test this hypothesis, three glucosinolates (**4**–**6**; see Fig. 1) were selected to demonstrate applicability with glucosinolates of commercial and synthetic origin bearing both natural and non-natural side chains. In addition, to ensure compatibility in both HPLC and UV–Vis spectroscopy analysis methods for the purpose of validation, all glucosinolates and resultant ITCs were required to have absorbance that scales linearly with analytical concentrations in aqueous buffer [26,29]. Sinigrin (**4**) was a commercially available natural glucosinolate that doubled as the standard to calibrate the specific activity of myrosinase [28]. Phenyl glucosinolate (**5**) was a synthetic non-natural glucosinolate; the hydrolysis kinetics for **5** has not been documented previously. Lastly, glucotropaeolin (**6**) was a synthetically prepared natural glucosinolate whose kinetics has been described in several accounts [36,37]. This article describes the development and validation of an HPLC method to analyze myrosinase-catalyzed conversion of glucosinolates to ITCs through a parallel kinetic evaluation of three glucosinolate substrates using HPLC and UV–Vis spectroscopy.

Materials and methods

General information

All reactions were carried out under nitrogen unless otherwise indicated. All reagents were obtained from available commercial sources and were used without further purification unless otherwise noted. The silica gel used in flash chromatography was 60 Å

and 230 to 400 mesh. Analytical thin-layer chromatography (TLC) was performed on Uniplate 250-μm silica gel plates with detection by UV light. Nuclear magnetic resonance (NMR) spectra were acquired on a Jeol ECS-400 400-MHz NMR spectrometer with multinuclear capability and a 24-sample autosampler with solvent as internal reference; the chemical shifts are reported in parts per million (ppm) in δ units. Infrared spectra were acquired on a Nicolet Avatar Fourier transform infrared (FTIR) instrument. UV–Vis spectroscopy experiments were conducted on a Shimadzu UV-2450 spectrometer fitted with a TCC-240A temperature-controlled cell chamber. HPLC experiments were conducted using an Agilent 1200 system with a degasser, photodiode array detector, and temperature-controlled autosampler. High-resolution mass spectroscopic data were obtained at the Mass Spectrometry and Analytical Proteomics Laboratory at the University of Kansas. Regression analyses were completed using the GraphPad Prism 6 software suite.

Preparation and characterization of ITCs and glucosinolates

The detailed experimental methods and spectral characterization for glucosinolates **5** and **6** and ITCs **8** and **9** are provided as supplementary data in the online supplementary material.

Calibration of myrosinase specific activity

The specific activity of commercial *S. alba* myrosinase (Sigma–Aldrich, cat. no. T4528) was determined using the established method [28]. Each final reaction mixture contained (−)-sinigrin stock (10.0 mM in ddH_2O, 50 μl), myrosinase stock (10 mg ml^{-1} in ddH_2O, 0–6 μl), and 0.1 M phosphate buffer at pH 7.4 (buffer A), with a total volume of 1.000 ml. Typical specific activity for 10 mg ml^{-1} myrosinase stock ranged from 0.5 to 1.1 U μl^{-1}.

UV–Vis kinetics assay

Molar absorptivities (M^{-1} cm^{-1}) of each analyte between 200 and 300 nm were determined from concentrations ranging from 1000 to 1.95 μM. Each hydrolysis reaction contained glucosinolate (1000–3.91 μM), myrosinase (**4**: 4.27 U; **5**: 14.52 U; **6**: 4.84 U), and buffer A, with a total volume of 1.000 ml. Solutions of glucosinolate in buffer A were stabilized at 37 °C in a 10-mm quartz cuvette for 15 min prior to the addition of enzyme. The absorbance was monitored at a single wavelength (**4**: 227, 235, 241 nm; **5**: 235, 254, 265, 274 nm; **6**: 227, 235, 241 nm) for 5 min. Linear changes in absorbance versus time were converted to initial reaction velocities (μM min^{-1}) using the difference in molar absorptivity between a glucosinolate and its ITC ($\Delta\varepsilon$, M^{-1} cm^{-1}).

General HPLC method

HPLC analysis was conducted with a Zorbax Eclipse XDB–C18 guard column (4.6 × 12.5 mm, 5 μM) and a Zorbax Eclipse XDB–C18 analytical column (4.6 × 150 mm, 5 μM), both at 25 °C, with a flow rate of 1 ml min^{-1} (ddH_2O with 0.1% [v/v] trifluoroacetic acid [TFA] at pump A; HPLC-grade CH_3CN with 0.1% [v/v] TFA at pump B). A linear gradient method was used: pre-run equilibration, 3.0% pump B; 0.00 min, 3.0% pump B; 3.00 min, 3.0% pump B; 8.00 min, 97.0% pump B; 8.01 min, 3.0% pump B; 13.00 min, 3.0% pump B. The autosampler was maintained at 37 °C. Following injection, the needle was washed with CH_3CN. The photodiode array detector used a 4-nm slit width and was autobalanced pre-run and post-run. Integration events were automated with the following features: tangent skim mode = standard, tail peak skim height ratio = 0.00, front peak skim height ratio = 0.00, skim valley ratio = 20.00, baseline correction = classical, peak-to-valley ratio = 500.00, slope sensitivity = 0.751, peak width = 0.121, area reject = 2.536, height reject = 0.176, and shoulders = off.

HPLC kinetics assay

From standards of glucosinolates **4** to **6** and ITCs **7** to **9** (1000 μM in buffer A, 37 °C) were performed seven injection volumes (1–100 μl) in triplicate. Standards were stabilized at 37 °C in the autosampler for at least 15 min prior to injection; to maintain sample integrity, ITC standards were freshly prepared from temperature-stabilized (37 °C) mixtures of buffer A and ITC stock immediately prior to injection [26]. Chromatograms were corrected for baseline drift through subtraction of a chromatogram following injection of an equal volume of buffer A and were independently analyzed at multiple wavelengths (**4**/**7**: 227, 235, 241 nm; **5**/**8**: 235, 254, 265, 274 nm; **6**/**9**: 227, 235, 241 nm). For each compound, the baseline-corrected peak integration area (mAU s) was linear between 0.25 and 12.50 nmol injected, with linear correlation coefficients (r^2) ranging from 0.9913 to 0.9997.

Hydrolysis reactions were performed in triplicate in an Agilent screw cap vial. Each hydrolysis reaction contained glucosinolate (1000–62.5 μM), myrosinase (**4**: 4.27 U; **5**: 14.52 U; **6**: 4.84 U), and buffer A, with a total volume of 1.000 ml. Solutions of glucosinolate in buffer A were stabilized at 37 °C in the autosampler for at least 15 min prior to the addition of enzyme. Reaction time was measured from the addition of myrosinase to the times of injection

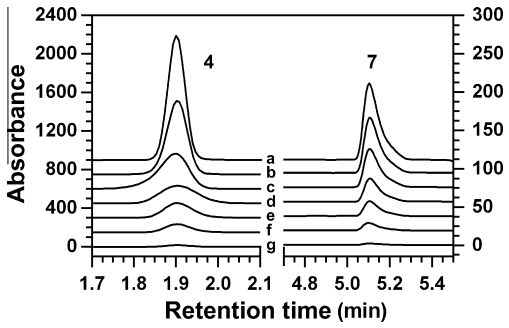

Fig.2. Representative baseline-corrected HPLC chromatograms following injection of **4** (retention time = 2.16 min) and **7** (retention time = 5.10 min) (235 nm). Chromatogram insets are provided for clarity; retention times not directly shown were baseline (<1 mAU). Chromatograms: (a) 12.5 nmol injected; (b) 8.75 nmol injected; (c) 6.25 nmol injected; (d) 3.75 nmol injected; (e) 2.50 nmol injected; (f) 1.25 nmol injected; (g) 0.25 nmol injected.

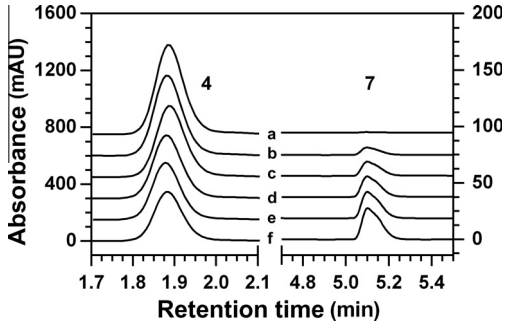

Fig.3. Representative HPLC chromatograms for the conversion of **4** ($[\mathbf{4}]_0$ = 250 μM, retention time = 2.16 min) to **7** (retention time = 5.10 min) with $[\mathbf{4}]_0$ = 250 μM and [Myr] = 4.27 U ml^{-1} (235 nm). Chromatogram insets are provided for clarity; retention times not directly shown were baseline (<1 mAU). Reaction time was measured from the addition of myrosinase to the times of injection (10 μl). Chromatograms: (a) t = 1.05 min; (b) t = 15.82 min; (c) t = 30.62 min; (d) t = 45.42 min; (e) t = 60.22 min; (f) t = 75.07 min.

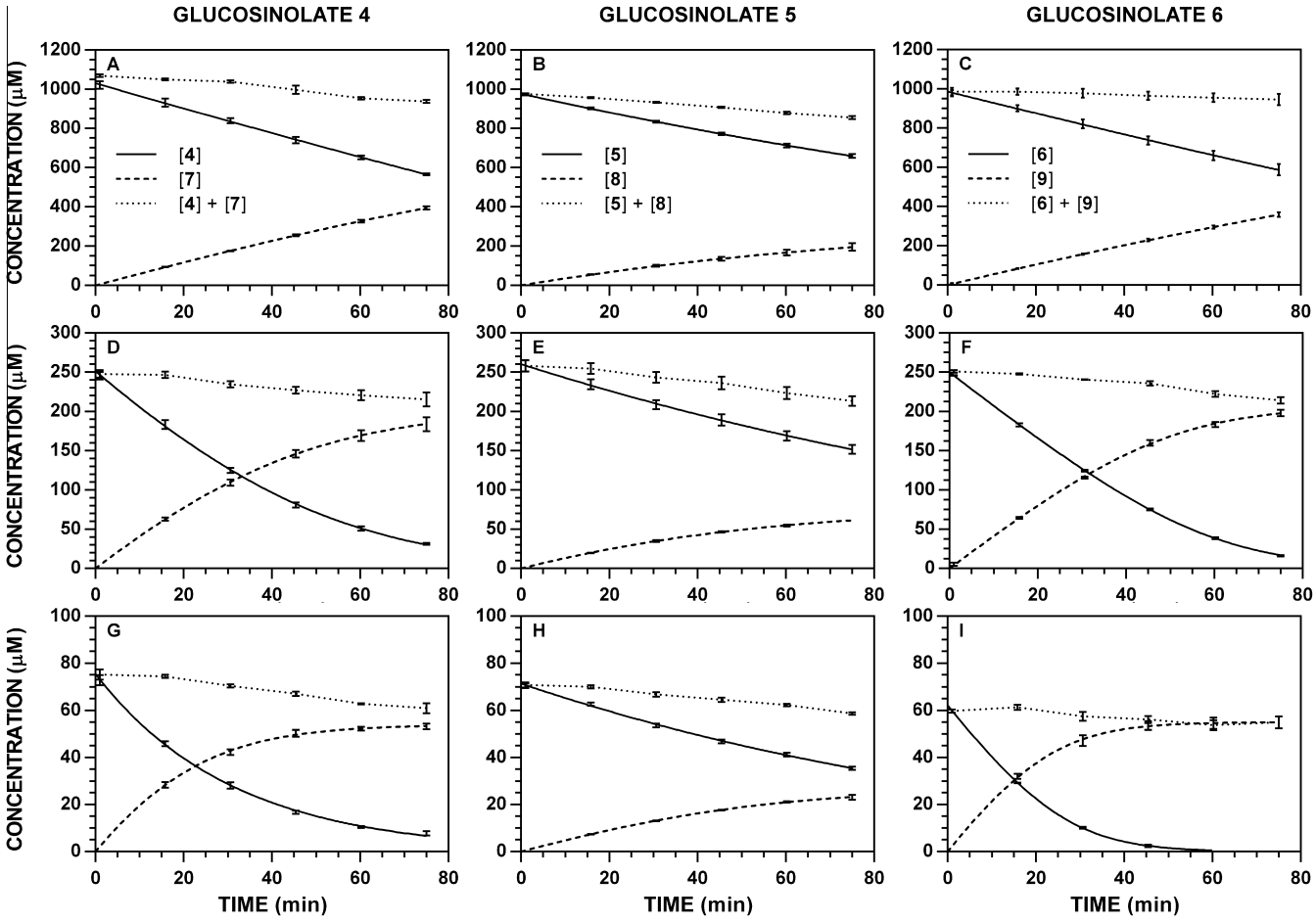

Fig.4. Representative HPLC-generated reaction progress curves for the conversion of glucosinolates to ITC at 37 °C (235 nm). The concentration of myrosinase was constant for a given substrate (**4**: 4.27 U ml^{-1}; **5**: 14.52 U ml^{-1}; **6**: 4.84 U ml^{-1}). Peak areas were used to determine [Gluc] and [ITC] at each timepoint, and the data ($n = 3$) were fitted to a reaction progress curve using nonlinear regression. The dotted line denotes the sum of [Gluc] + [ITC] at each timepoint, and its slope represents ITC loss over time. Reaction progress curves for each $[Gluc]_0$ – wavelength combination are available as supplementary material. Panels: (A) $[\mathbf{4}]_0 = 1000$ μM; (B) $[\mathbf{5}]_0 = 1000$ μM; (C) $[\mathbf{6}]_0 = 1000$ μM; (D) $[\mathbf{4}]_0 = 250$ μM; (E) $[\mathbf{5}]_0 = 250$ μM; (F) $[\mathbf{6}]_0 = 250$ μM; (G) $[\mathbf{4}]_0 = 62.5$ μM; (H) $[\mathbf{5}]_0 = 62.5$ μM; (I) $[\mathbf{6}]_0 = 62.5$ μM.

(10 μl), which occurred at 1.05, 15.82, 30.62, 45.42, 60.22, and 75.07 min.

Analyte concentrations were calculated from the standard curves and were used to fit reaction progress curves via nonlinear regression in GraphPad Prism 6.0. Glucosinolate reaction progress curves ($[Gluc]_t$) were fitted to a temporal closed-form solution of the Michaelis–Menten equation incorporating the Lambert $W(x)$ function (Goličnik's Eq. 11) [38]; ITC reaction progress curves ($[ITC]_t$) were similarly fitted (Goličnik's Eq. 7) [38]. Initial variable values for nonlinear regression were $[Gluc]_0 = 500$ μM, $K_m = 1.0$ μM, and $V_{max} = 8.0$ μM min^{-1}. In GraphPad Prism 6.0, the first derivative of each reaction progress curve was generated with smoothing (four neighbors on each side, second-order polynomial), and initial reaction velocities (V_0 values) were obtained from this curve at $t = 0$ min.

Michaelis–Menten analysis

Velocity data generated by both UV–Vis and HPLC methods were fitted to the Michaelis–Menten equation using nonlinear regression in GraphPad Prism 6.0 [38]. Initial variable values for nonlinear regression were $K_m = 1.0$ μM and $V_{max} = 1.0$ μM min^{-1}; K_m was restrained to ensure that the converged value was greater than zero. Best-fit values for K_m and V_{max} were reported with correlation coefficients (r^2, range = 0.9588–0.9990).

Results and discussion

Myrosinase kinetics assay (UV–Vis)

UV–Vis spectroscopy was used to confirm that the absorbance of all analytes scaled linearly with concentration in aqueous buffer, to determine the specific activity of myrosinase, and to evaluate hydrolysis kinetics; these methods were based on established protocols, with minor alterations to accommodate congruency with the HPLC assay [28]. The wavelengths selected for kinetic analysis corresponded to either a glucosinolate λ_{max}, an ITC λ_{max}, an absorbance shoulder common to all glucosinolates (235 nm), or a standard aromatic absorbance (254 nm). The specific activity of myrosinase was determined spectrophotometrically at 227 nm using **4** as substrate [26,28]. To maintain consistency with past standardization methods, $\Delta\varepsilon_{227} = 6458$ M^{-1} cm^{-1} was used to calculate initial reaction velocities and one unit of myrosinase was defined as the amount of enzyme able to hydrolyze 1 nmol of **4** per minute at pH 7.4 and 37 °C when the initial concentration of **4** ($[\mathbf{4}]_0$) was 250 μM [28].

Initial reaction velocities for the myrosinase-catalyzed conversion of glucosinolates to ITCs were determined using a modification of the established UV–Vis protocol [26,28]. Reaction velocities (V_0 values, μM min^{-1}) were calculated from plots of absorbance versus time using the difference in the molar

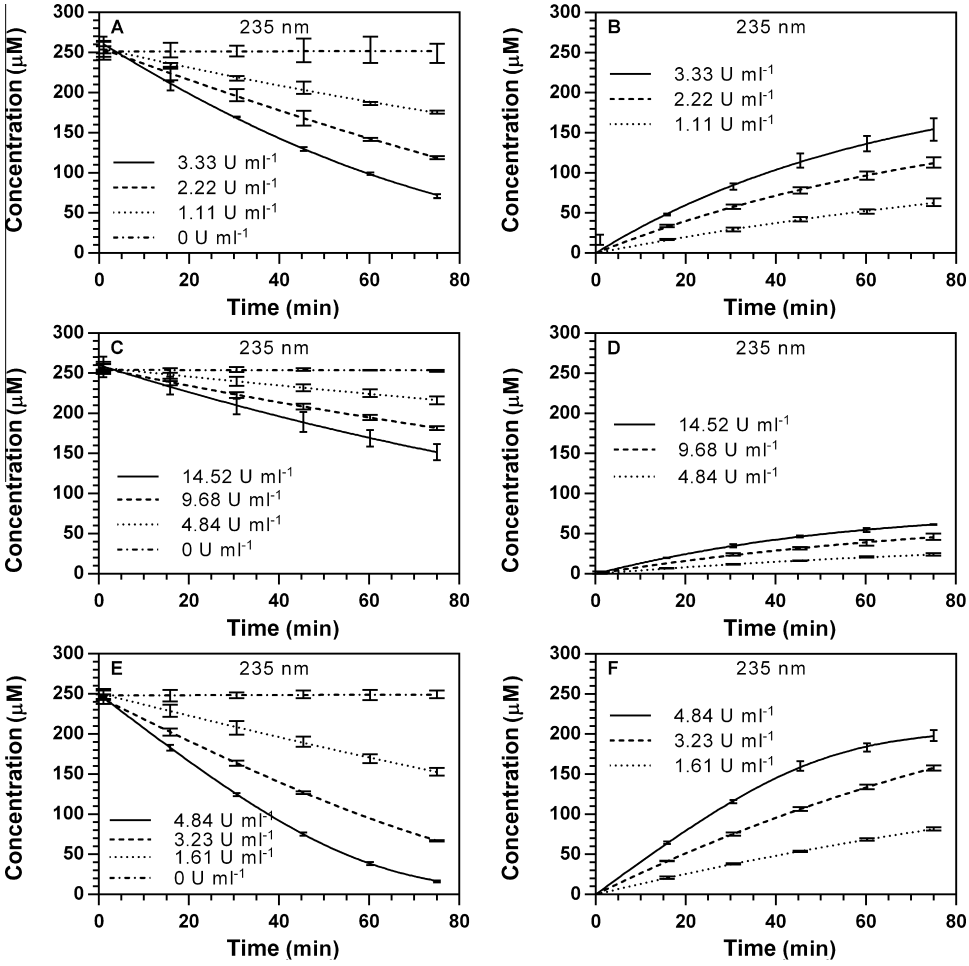

Fig.5. Enzyme dependence on HPLC reaction progress curves for $[Gluc]_t$ and $[ITC]_t$ at 37 °C ($[Gluc]_0$ = 250 μM, 235 nm). Peak areas were used to determine [Gluc] and [ITC] at each timepoint, and the data (n = 3) were fitted to a reaction progress curve using nonlinear regression. Progress curves for other wavelength–substrate combinations are available as supplementary material. Panels: (A) $[\mathbf{4}]_t$; (B) $[\mathbf{7}]_t$; (C) $[\mathbf{5}]_t$; (D) $[\mathbf{8}]_t$; (E) $[\mathbf{6}]_t$; (F) $[\mathbf{9}]_t$.

absorptivity between ITC and glucosinolate ($\Delta\varepsilon = \varepsilon_{(ITC)} - \varepsilon_{(glucosinolate)}$); these velocities are available as supplementary material. The V_0 values were relatively consistent between wavelengths for a given initial concentration of glucosinolate ($[Gluc]_0$) and, as expected, V_0 values were proportional to $[Gluc]_0$. A second set of kinetic studies was conducted with constant $[Gluc]_0$ (250 μM) using four relative concentrations of myrosinase [Myr]: 100, 67, 33, and 0% of a maximum (**4**: 3.33 U ml^{-1}; **5**: 14.52 U ml^{-1}; **6**: 4.84 U ml^{-1}). These V_0 data (see Table SD-3 in supplementary material) were also proportional to [Myr]; in the absence of myrosinase, the V_0 was minimal.

Myrosinase kinetics assay (HPLC)

Parallel kinetic analysis was conducted using a reverse-phase HPLC method that incorporated several improvements over prior HPLC methodology [26]. A distinct advantage of using HPLC to analyze reaction kinetics was its ability to chromatographically separate reactant (glucosinolate) and product (ITC) and to independently and directly quantify their concentrations versus time. Early in method development, other low-percentage glucosinolate hydrolysis products (e.g., nitrile, thiocyanates) and ITC-derived amines (via hydrolysis) were analyzed using the HPLC method with the expectation that they may be observed as minor products during kinetic analysis (data not shown). Surprisingly, peaks corresponding to these other potential products were not observed in hydrolysis chromatograms; consequently, subsequent data analysis was limited to glucosinolates and the ITCs, which appeared to be the only detectable hydrolysis product.

A challenge in developing an HPLC method to simultaneously evaluate glucosinolates and ITCs was the diverse polarity of these substances and finding a solvent gradient that provided resolution with minimal compromise to efficiency. Maintaining an isocratic polar mobile phase for 3 min provided sufficient resolution of glucosinolates from the void volume, after which a gradient to nonpolar mobile phase over 5 min resulted in elution of ITCs. Although a steeper gradient would have decreased total time per injection, inconsistent mixing of rapidly changing elution solvents had a negative impact on the ability to apply a consistent and reproducible baseline correction. The described 8-min method provided reproducible retention times for glucosinolates between 1.90 and 3.32 min and for ITCs between 5.12 and 5.73 min (Fig. 2); a 5-min reequilibration of initial mobile phase and the unavoidable autosampler–computer lag between injections kept the total time per injection under 15 min, a significant improvement over previous HPLC methods [26]. Chromatograms generated throughout an enzyme-catalyzed transformation provided the ability to observe hydrolysis of glucosinolate and formation of ITC (Fig. 3).

Although linear regression directly provided V_0 using UV–Vis spectroscopy, HPLC-generated $[Gluc]_t$ and $[ITC]_t$ plots were nonlinear and V_0 values were determined through implementation of reaction progress curves [32–34], where rates of glucosinolate hydrolysis ($\Delta[Gluc]\,\Delta t^{-1}$) and ITC formation ($\Delta[ITC]_{obs}\,\Delta t^{-1}$) were obtained from their slopes at t = 0 min (see Tables SD-5 and SD-6 in

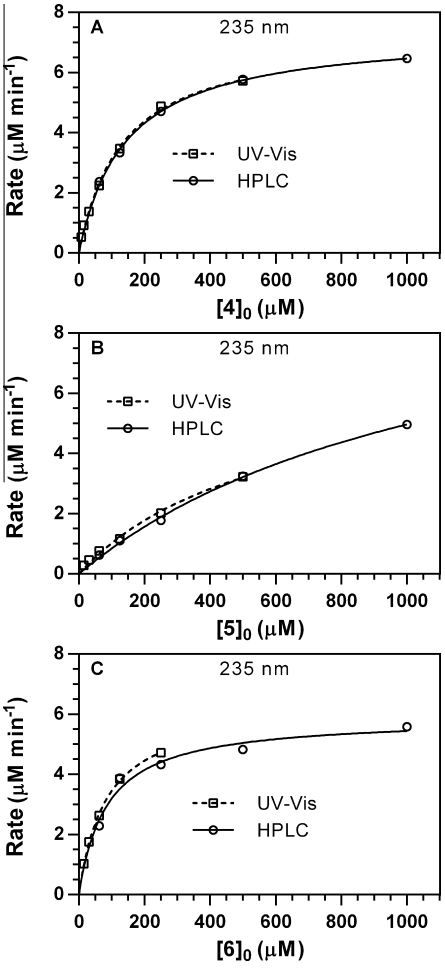

Fig.6. Michaelis–Menten plots for V_0 versus $[Gluc]_0$ data from UV–Vis and HPLC methods (37 °C, 235 nm). The concentration of myrosinase was constant for a given substrate (**4**: 4.27 U ml^{-1}; **5**: 14.52 U ml^{-1}; **6**: 4.84 U ml^{-1}). Michaelis–Menten plots for other wavelength–substrate combinations are available as supplementary material. Panels: (A) **4** to **7**; (B) **5** to **8**; (C) **6** to **9**.

supplementary material). Reaction progress curves to describe $[Gluc]_t$ were generated using nonlinear regression with a closed-form solution of the Michaelis–Menten equation (Goličnik's Eq. 3) employing the Lambert $W(x)$ function (Goličnik's Eq. 11) [38]. Representative progress curves monitored at 235 nm for the conversion of **4** to **7**, **5** to **8**, and **6** to **9** are provided (Fig. 4); progress curves for all other substrate/wavelength combinations are available as supplementary material. Reaction progress curves to describe $[ITC]_t$ (Fig. 4, dashed lines) were generated using an alternate approximation of the Michaelis–Menten equation (Goličnik's Eq. 7) [38]. The $W(x)$ approximation did not provide consistent $[ITC]_t$ progress curves that fit the data, likely due to complications arising from the competing rate of ITC loss ($\Delta[ITC]_{loss}\ \Delta t^{-1}$) [26]. Despite the reduction in total reaction time from 9 h [26] to 75 min, appreciable ITC loss was still observed; this effect was particularly noticeable at low $[Gluc]_0$ where negative $\Delta[ITC]_{obs}\ \Delta t^{-1}$ were observed at reaction times following complete consumption of glucosinolate. As documented previously, HPLC chromatograms did not indicate the presence of any noticeable degradation products [21,39–41] and additional evidence toward rationalizing this loss was not identified. To explore this phenomenon, the sum of [Gluc] + [ITC] at each timepoint (Fig. 4, dotted lines) was calculated as a representation of the detectable concentration balance of each transformation. Given the 1:1 reaction stoichiometry, this sum should equal $[Gluc]_0$ at all points; however, this sum decreases over time, representing a net rate of detectable ITC loss. Further experimentation will be required to rationalize this observed loss and will be reported in due course.

HPLC-monitored hydrolysis reactions were also conducted to test the effect of [Myr] on V_0 with regard to both $\Delta[Gluc]\ \Delta t^{-1}$ and $\Delta[ITC]_{obs}\ \Delta t^{-1}$. To maintain consistency with the corresponding UV–Vis spectroscopy experiments, substrate concentration was constant ($[Gluc]_0$ = 250 μM) and the same relative array of [Myr] was used (100, 67, 33, and 0% of maximum; **4**: 3.33 U ml^{-1}; **5**: 14.52 U ml^{-1}; **6**: 4.84 U ml^{-1}). Representative progress curves at 235 nm are depicted in Fig. 5; progress curves for all other substrate/wavelength combinations are available as supplementary material. As before, both $[Gluc]_t$ and $[ITC]_t$ data demonstrate that [Myr] was proportional to V_0 (see supplementary material); in the absence of myrosinase, the detectable $[Gluc]_t$ and $[ITC]_t$ did not change over time.

Comparison of UV–Vis and HPLC methods

Myrosinase follows the Michaelis–Menten mechanism [28], where V_0 is dependent on $[Gluc]_0$, the Michaelis–Menten constant (K_m), and the maximum velocity (V_{max}) [38]. Using nonlinear

Table 1
Michaelis–Menten kinetic constants for the action of *Sinapis alba* myrosinase on glucosinolates.

Entry	λ (nm)	K_m (μM)		V_{max} (μM min^{-1})		V_{max} [Myr]$^{-1}$ (min^{-1})		Relative rate (%)	
		UV–Vis	HPLC	UV–Vis	HPLC	UV–Vis	HPLC	UV–Vis	HPLC
4 to **7**	227	198 ± 29	233 ± 41	8.16 ± 0.67	8.78 ± 0.57	1.91[a]	2.06	100	108
	235	132 ± 10	142 ± 8	7.29 ± 022	7.38 ± 0.13	1.71	1.73	89	90
	241	122 ± 19	147 ± 27	8.14 ± 0.48	7.68 ± 0.45	1.91	1.80	100	94
	Pooled	149 ± 21	168 ± 17	7.94 ± 0.48	7.88 ± 0.26	1.86	1.85	97	97
5 to **8**	235	569 ± 117	1187 ± 155	6.84 ± 0.88	10.87 ± 0.90	0.47	0.75	25	39
	254	3185 ± 3061	1136 ± 115	20.10 ± 17.09	10.24 ± 0.87	1.38	0.71	72	37
	265	2070 ± 329	1204 ± 170	15.03 ± 1.75	10.86 ± 0.97	1.04	0.75	54	39
	274	1822 ± 211	1108 ± 120	14.10 ± 1.16	10.45 ± 0.70	0.97	0.72	51	38
	Pooled	1709 ± 302	1157 ± 70	13.33 ± 1.72	10.60 ± 0.40	0.92	0.73	48	38
6 to **9**	227	97.8 ± 7.6	83.9 ± 8.7	7.16 ± 0.25	5.83 ± 0.15	1.48	1.20	77	63
	235	82.6 ± 4.5	84.6 ± 17.4	6.29 ± 0.14	5.90 ± 0.31	1.30	1.22	68	64
	241	57.8 ± 5.0	105.2 ± 9.0	5.79 ± 0.15	6.10 ± 0.14	1.20	1.26	63	66
	Pooled	72.0 ± 5.7	90.6 ± 6.8	6.15 ± 0.18	5.93 ± 0.12	1.27	1.23	66	64

Note. Results were independently evaluated using both UV–Vis spectroscopy and HPLC methods at multiple wavelengths; regression analysis of pooled wavelength data for each glucosinolate/ITC pair are also included. The Michaelis–Menten constant ± standard error (K_m, μM) and maximum velocity ± standard error (V_{max}, μM min^{-1}) are shown. Calculated V_{max} values were normalized to the concentration of myrosinase ([Myr], U ml^{-1}) to yield normalized rate constants (min^{-1}) and relative percentage rates versus **4** (UV–Vis, 227 nm).

[a] Point of reference for the relative maximum rates of hydrolysis.

Table 2
Specific activities (V_0, min^{-1}) for the hydrolysis of glucosinolates ($[Gluc]_0$ = 250 μM) by *Sinapis alba* myrosinase determined in parallel using UV–Vis spectroscopy and HPLC methods.

Entry	λ (nm)	V_0 $[Myr]^{-1}$ (min^{-1})			Relative specific activity (%)		
		UV–Vis	HPLC–$[Gluc]_t$	HPLC–$[ITC]_t$	UV–Vis	HPLC–$[Gluc]_t$	HPLC–$[ITC]_t$
4 to **7**	227	0.94 ± 0.04[a]	0.92 ± 0.01	1.04 ± 0.06	100	98	111
	235	1.02 ± 0.02	1.00 ± 0.08	1.04 ± 0.02	109	106	111
	241	1.20 ± 0.05	1.08 ± 0.02	0.98 ± 0.02	128	115	104
5 to **8**	235	0.14 ± 0.01	0.12 ± 0.00	0.10 ± 0.00	15	13	11
	254	0.10 ± 0.00	0.13 ± 0.00	0.11 ± 0.00	11	14	12
	265	0.11 ± 0.00	0.13 ± 0.01	0.11 ± 0.00	12	14	12
	274	0.12 ± 0.01	0.13 ± 0.00	0.11 ± 0.00	13	14	12
6 to **9**	227	1.00 ± 0.02	0.88 ± 0.02	0.76 ± 0.05	106	94	81
	235	0.98 ± 0.03	0.88 ± 0.01	0.86 ± 0.00	104	94	91
	241	0.98 ± 0.07	0.88 ± 0.01	0.78 ± 0.05	104	94	83

Note. HPLC data for $[Gluc]_t$ (HPLC–$[Gluc]_t$) and $[ITC]_t$ (HPLC–$[ITC]_t$) were independently tracked. Specific activities were normalized to the specific activity of **4** (UV–Vis, 227 nm).
[a] Point of reference for relative specific activities at $[Gluc]_0$ = 250 μM.

regression, Michaelis–Menten curves were independently generated for each wavelength–glucosinolate–method combination [32]. Representative Michaelis–Menten plots for the hydrolysis of **4** to **6** (235 nm) generated from both UV–Vis and HPLC experiments are depicted in Fig. 6; analogous plots for other wavelengths are available as supplementary material. Despite the different limits of sensitivity for the analytical range between UV–Vis spectroscopy and HPLC, the Michaelis–Menten curves from the two methods are consistent with one another; each Michaelis–Menten curve was fit with a high correlation coefficient (UV–Vis: $r^2 > 0.9890$; HPLC: $r^2 > 0.9588$; see Table 2). Converged K_m and V_{max} values across independently monitored wavelengths for a given substrate were congruent; when independently–monitored wavelength V_0 and $[Gluc]_0$ data were treated as separate trials, pooled per substrate, and subjected to Michaelis–Menten analysis (see supplementary material), a similar high correlation coefficient (UV–Vis: $r^2 > 0.9716$; HPLC: $r^2 > 0.9723$) was observed. This comparison suggests that kinetic analysis of glucosinolates can be conducted at a variety of wavelengths without compromising experimental results, supporting the hypothesis that both analytical methods provide data of equivalent quality and precision.

These studies provided a complete comprehensive kinetic characterization of glucosinolates **4** to **6** with *S. alba* myrosinase. Although **4** has been used as a substrate for myrosinase in several studies, variances in the organismal source of myrosinase, isozyme, level of purity and the resultant effects on intrinsic activity, pH, and temperature limit the ability for direct comparison with known standard values [42]. In this study, the K_m of **4** ranged from 122 to 233 μM and was supportive of prior findings: 117 μM (*S. alba*) [26], 359 μM (*Brevicoryne brassicae*) [37], and 410 μM (*B. brassicae*) [36]. For **5**, the UV–Vis-derived K_m showed greater variance (K_m = 569–3185 μM) and the HPLC data were much more consistent (K_m = 1108–1204 μM); this study represents the first documented K_m for non-natural glucosinolate **5**. Glucosinolate **6** demonstrated a K_m range of 57 to 105 μM, supportive of previous accounts: K_m = 161 μM (*B. brassicae*) [37], K_m = 520 μM (*B. brassicae*) [36], and K_m = 125 μM (*S. alba*) [27]. Structurally, the combination of conformational flexibility in the side chain in **4** and **6** and the reduced steric impact near the thiohydroximate may provide lower K_m versus the rigid phenyl group in **5**.

Rather than determining k_{cat}, which is heavily influenced by the purity and intrinsic activity of enzyme, V_{max} (μM min^{-1}) was normalized to [Myr], expressed in terms of its specific activity (U μl^{-1}). Because the specific activity of each enzyme stock was determined prior to kinetic analysis and was based on a common standard ($[\mathbf{4}]_0$ = 250 μM, 227 nm), normalization provided the ability to directly compare the catalytic efficiency of substrates independent of the differences in intrinsic activity for enzyme stocks that were used. Unsurprisingly, **4** demonstrated a relative maximum velocity of 89 to 108% versus itself as standard. Similarly, based on the more consistent HPLC data, the catalytic rates of hydrolysis of **5** and **6** appear to be 37 to 39% and 63 to 66% the rate for **4**, respectively; previous accounts have described the relative maximum velocity of **6** versus **4** as 34% [37] and 63% [36].

Analysis of specific activity plots allowed comparison of three methods of detection: UV–Vis spectroscopy and HPLC (independent V_0 from both $[Gluc]_t$ and $[ITC]_t$); representative plots conducted at 235 nm are depicted in Fig. 7. A linear correlation ($r^2 > 0.9884$) was observed between V_0 and [Myr], including data derived from $[ITC]_t$ whose observed velocities were affected $\Delta[ITC]_{loss}\,\Delta t^{-1}$. Specific activities of each substrate ($[Gluc]_0$ = 250 μM) and normalized specific activities versus the standard ($[\mathbf{4}]_0$ = 250 μM, 227 nm) are provided in Table 2. Specific activities were consistent for each glucosinolate across both the method of detection and the wavelength monitored. Although a direct proportionality between normalized specific activities and normalized maximum rates (Table 1) was impossible due to the mathematical contributions of K_m, the normalized specific activities demonstrate similar relative velocity trends versus the normalized V_{max}; normalized specific activities of **4** were nearly 100% versus itself, those of **5** were approximately an order of magnitude less than **4**, and those of **6** were 60 to 80% lower compared with **4**.

Both UV–Vis and HPLC methods of kinetic analysis offer advantages and disadvantages with regard to each other. Advantages of UV–Vis spectroscopy include its ease of use, the general availability of analytical-grade instrumentation, and the rapid rate of data acquisition. However, elucidation of kinetic parameters requires either prior knowledge of the UV–Vis properties of all reactants and products or purified samples for standardization; in cases where the products are unknown, unavailable, or formed in a complex mixture, accurate kinetic analysis would be limited. Furthermore, in relation to a key premise of this work, UV–Vis spectroscopy might not be amenable for direct detection of glucosinolate/ITC pairs whose absorbance does not scale linearly with concentration in aqueous buffer. By comparison, advantages of the HPLC approach lie in its ability to chromatographically separate and independently evaluate substrates and products, its ability to incorporate elements of automation, and its ability to accommodate glucosinolate/ITC systems with limited aqueous solubility. In contrast, limitations of the HPLC method may include accessibility to instrumentation, increased cost of materials (e.g., elution solvents), and the length of time required to generate data;

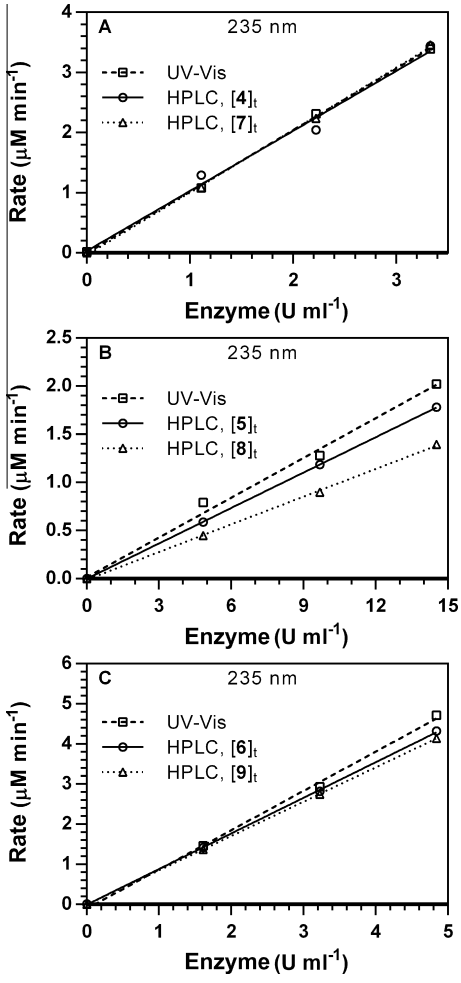

Fig.7. Specific activity plots from UV–Vis and HPLC methods (37 °C, $[Gluc]_0$ = 250 - μM). HPLC data for $[Gluc]_t$ (HPLC–$[Gluc]_t$) and $[ITC]_t$ (HPLC–$[ITC]_t$) were independently tracked. Plots for other wavelength–substrate combinations are available as supplementary material. Panels: (A) **4** to **7**; (B) **5** to **8**; (C) **6** to **9**.

this latter point may be partially offset by instrument automation. Because each 75-min injection sequence requires approximately 5 min of hands-on human interaction to initiate the experiment, triplicate analysis of five initial substrate concentrations for a single glucosinolate would require 75 min of human work spaced throughout the 1350 min of automated instrument use (94% time efficiency).

Conclusions

The central hypothesis of this work was that the kinetic data produced by the HPLC assay would parallel the data acquired using traditional UV–Vis methods, supporting the interchangeable use of either analytical technique in future kinetic evaluations of both natural and non-natural glucosinolates. The results of our parallel evaluation demonstrated that kinetic data were consistent between methods and that all three glucosinolates responded similarly to both Michaelis–Menten and specific activity analysis independent of the wavelength monitored. The complete kinetic characterization three glucosinolates with *S. alba* myrosinase was accomplished with results that were consistent with previous reports; for non-natural glucosinolate **5**, this represents its first documented kinetic assessment. Together, these data support the continued use of the described HPLC kinetics approach for the evaluation of glucosinolate hydrolysis.

Outside the realm of myrosinase kinetic evaluation, the broader impact of this work lies both in the described HPLC method and the application of nonlinear reaction progress curves to elucidate V_0. Using a multistep mobile phase gradient provides the opportunity to reproducibly resolve analytes with varied physical properties with moderate injection efficiency (~15 min per injection). At substrate concentrations below enzyme saturation, HPLC reaction progress plots become increasingly nonlinear. Fitting this type of data to an appropriate nonlinear curve, such as the solution to the Michaelis–Menten equation used in this account, would provide the flexibility to evaluate V_0 under a wider array of experimental conditions. Furthermore, as others have described [32,43], with enough data points it may be feasible to calculate Michaelis–Menten kinetic parameters directly from nonlinear analysis of a single initial concentration of substrate, a feature that would undoubtedly provide substantial time and cost savings when evaluating enzyme kinetics.

Acknowledgments

This research was supported by an Institutional Development Award (IDeA) from the National Institute of General Medical Sciences of the National Institutes of Health under grant P20GM103443. The content is solely the responsibility of the authors and does not necessarily represent the official views of the National Institutes of Health. This research was also supported by the Sanford Program for Undergraduate Research. We extend our thanks to Brandon Gustafson, the faculty and staff in the Department of Chemistry at Augustana College, and the Mass Spectrometry and Analytical Proteomics Laboratory at the University of Kansas.

Appendix A. Supplementary data

Supplementary data associated with this article can be found, in the online version, at http://dx.doi.org/10.1016/j.ab.2014.07.017.

References

[1] X. Chen, J. Liu, S.-Y. Chen, Sulforaphane protects against ethanol-induced oxidative stress and apoptosis in neural crest cells by the induction of Nrf2-mediated antioxidant response, Br. J. Pharmacol. 169 (2013) 437–448.
[2] A.L. Benedict, E.V. Knatko, A.T. Dinkova-Kostova, The indirect antioxidant sulforaphane protects against thiopurine-mediated photooxidative stress, Carcinogenesis 33 (2012) 2457–2466.
[3] G.S. Kumar, V. Ramakrishnan, N. Madhusudhanan, M.P. Balasubramanian, Antioxidant activity of allyl isothiocyanate [AITC] against *N*-nitrosodiethylamine induced experimental liver carcinogenesis, J. Pharm. Res. 4 (2011) 3690–3694.
[4] P. Thejass, G. Kuttan, Allyl isothiocyanate (AITC) and phenylisothiocyanate (PITC) inhibit tumor-specific angiogenesis by downregulating nitric oxide (NO) and tumour necrosis factor–alpha (TNF-α) production, Nitric Oxide 16 (2007) 247–257.
[5] H.-J. Park, S.-J. Kim, S.-J. Park, S.-H. Eom, G.-J. Gu, S.H. Kim, H.-S. Youn, Phenethyl isothiocyanate regulates inflammation through suppression of the TRIF-dependent signaling pathway of Toll-like receptors, Life Sci. 92 (2013) 793–798.
[6] T. Uto, D.-X. Hou, O. Morinaga, Y. Shoyama, Molecular mechanisms underlying anti-inflammatory action of 6-(methylsulfinyl)hexyl isothiocyanate derived from wasabi (*Wasabia japonica*), Adv. Pharmacol. Sci. 2012 (2012) 614046.
[7] A.E. Wagner, C. Boesch-Saadatmandi, J. Dose, G. Schultheiss, G. Rimbach, Anti-inflammatory potential of allyl-isothiocyanate: role of Nrf2, NF-κB, and microRNA-155, J. Cell. Mol. Med. 16 (2012) 836–843.
[8] A. Sofrata, E.M. Santangelo, M. Azeem, A.-K. Borg-Karlson, A. Gustafsson, K. Putsep, Benzyl isothiocyanate, a major component from the roots of *Salvadora persica*, is highly active against gram-negative bacteria, PLoS ONE 6 (2011) e23045.
[9] H.W. Kim, C.H. Lee, M.-G. Kim, H.-S. Lee, Antibacterial activities of phenethylisothiocyanate and its derivatives against human oral pathogens, J. Korean Soc. Appl. Biol. Chem. 52 (2009) 555–559.

[10] H. Masuda, Function of omega-methylthioalkyl isothiocyanates in wasabi (*Wasabia japonica* Matsumura), Koryo 239 (2008) 89–96.
[11] G. Brandi, G. Amagliani, G.F. Schiavano, M. De Santi, M. Sisti, Activity of *Brassica oleracea* leaf juice on foodborne pathogenic bacteria, J. Food Prot. 69 (2006) 2274–2279.
[12] I. Azalez, G. Meca, L. Manyes, M. Fernandez-Franzon, Antifungal activity of gaseous allyl, benzyl, and phenyl isothiocyanate in vitro and their use for fumonisins reduction in bread, Food Control 32 (2013) 428–434.
[13] E.P. Padia, L.T. Solls, R.M. Levida, C.-C. Shen, C.Y. Ragassa, Antimicrobial isothiocyanates from the seeds of *Moringa oleifera* Lam, Zeitschrift für Naturforschung [J. Biosci.] 67 (2013) 557–564.
[14] J.D. Clarke, A. Hsu, Z. Yu, R.H. Dashwood, E. Ho, Differential effects of sulforaphane on histone deacetylases, cell cycle arrest, and apoptosis in normal prostate cells versus hyperplastic and cancerous prostate cells, Mol. Nutr. Food Res. 55 (2011) 999–1009.
[15] E. Rudolf, M. Cervinka, Sulforaphane induces cytotoxicity and lysosome- and mitochondria-dependent cell death in colon cancer cells with deleted p53, Toxicol. In Vitro 25 (2011) 1302–1309.
[16] S.M. Meeran, A. Ahmed, T.O. Tollefsbol, Epigenetic targets of bioactive dietary components for cancer prevention and therapy, Clin. Epigenet. 1 (2010) 101–116.
[17] A.T. Dinkova-Kostova, The effectiveness of the isothiocyanate sulforaphane in chemoprotection, Acta Horticult. 867 (2010) 27–36.
[18] D.B. Clarke, Glucosinolates, structures, and analysis in food, Anal. Methods 2 (2010) 310–325.
[19] B.A. Halkier, J. Gershenzon, Biology and biochemistry of glucosinolates, Annu. Rev. Plant Biol. 57 (2006) 303–333.
[20] M. Uchiyama, Synthesis and properties of *N*-acyl analogs of mustard oil glucoside and their enzymic cleavage by myrosinase, Nippon Nogei Kagaku Kaishi 37 (1963) 543–547.
[21] V. Gil, A.J. MacLeod, The effects of pH on glucosinolate degradation by a thioglucoside glucohydrolase preparation, Phytochemistry 19 (1980) 2547–2551.
[22] R. Iori, P. Rollin, H. Streicher, J. Thiem, S. Palmieri, The myrosinase–glucosinolate interaction mechanism studied using some synthetic competitive inhibitors, FEBS Lett. 385 (1996) 87–90.
[23] A. Bourderioux, M. Lefoix, D. Gueyrard, A. Tatibouet, S. Cottaz, S. Arzt, W.P. Burmeister, P. Rollin, The glucosinolate–myrosinase system: new insights into enzyme–substrate interactions by use of simplified inhibitors, Org. Biomol. Chem. 3 (2005) 1872–1879.
[24] A. Besle, X. Brazzolotto, A. Tatibouet, D. Cerniauskaite, E. Gallienne, P. Rollin, W.P. Burmeister, A micromolar O-sulfated thiohydroximate inhibitor bound to plant myrosinase, Acta Crystallogr. F 66 (2010) 152–156.
[25] X. Wang, A.J. Di Pasqua, S. Govind, E. McCracken, C. Hong, L. Mi, Y. Mao, J.Y. Wu, Y. Tomita, J.C. Woodrick, R.L. Fine, F.L. Chung, Selective depletion of mutant p53 by cancer chemopreventive isothiocyanates and their structure–activity relationships, J. Med. Chem. 54 (2011) 809–816.
[26] J.R. Mays, R.L. Weller-Roska, S. Sarfaraz, H. Mukhtar, S.R. Rajski, Identification, synthesis, and enzymology of non-natural glucosinolate chemopreventive candidates, ChemBioChem 9 (2008) 729–747.
[27] R. Nehmé, H. Nehmé, G. Roux, D. Cerniauskaite, P. Morin, P. Rollin, A. Tatibouët, Contactless conductivity detection for screening myrosinase substrates by capillary electrophoresis, Anal. Chim. Acta 807 (2014) 153–158.
[28] S. Palmieri, O. Leoni, R. Iori, A steady-state kinetics study of myrosinase with direct ultraviolet spectrophotometric assay, Anal. Biochem. 123 (1982) 320–324.
[29] J.R. Mays, Synthetic and Biological Studies Directed at the Development of New HDAC-Inhibiting Prodrugs, University of Wisconsin-Madison, 2007.
[30] M. Patel, M.M. Vasaya, D. Asker, R.B. Parsons, HPLC–UV method for measuring nicotinamide *N*-methyltransferase activity in biological samples: evidence for substrate inhibition kinetics, J. Chromatogr. B 921 (922) (2013) 87–95.
[31] L.C. Bui, L. Tabouy, F. Busi, J.-M. Dupret, N. Janel, C. Planque, J.-M. Delabar, F. Rodrigues-Lima, J. Dairou, A high-performance liquid chromatography assay for Dyrk1a, a Down syndrome-associated kinase, Anal. Biochem. 449 (2014) 172–178.
[32] M. Goličnik, The integrated Michaelis–Menten rate equation: deja vu or vu jade?, J Enzyme Inhib. Med. Chem. 28 (2013) 879–893.
[33] M.V. Putz, A.-M. Lacrama, V. Ostafe, Full analytic progress curves of enzymic reactions in vitro, Int. J. Mol. Sci. 7 (2006) 469–484.
[34] R.G. Duggleby, Estimation of the initial velocity of enzyme-catalyzed reactions by non-linear regression analysis of progress curves, Biochem. J. 228 (1985) 55–60.
[35] C.T. Goudar, An explicit expression for determining cometabolism kinetics using progress curve analysis, J. Biotechnol. 159 (2012) 56–60.
[36] B. Pontoppidan, B. Ekbom, S. Eriksson, J. Meijer, Purification and characterization of myrosinase from the cabbage aphid (*Brevicoryne brassicae*), a brassica herbivore, Eur. J. Biochem. 268 (2001) 1041–1048.
[37] F. Francis, G. Lognay, J.-P. Wathelet, E. Haubruge, Characterization of aphid myrosinase and degradation studies of glucosinolates, Arch. Insect Biochem. Physiol. 50 (2002) 173–182.
[38] M. Goličnik, Explicit reformulations of time-dependent solution for a Michaelis–Menten enzyme reaction model, Anal. Biochem. 406 (2010) 94–96.
[39] L. Song, R. Iori, P.J. Thornalley, Purification of major glucosinolates from *Brassicaceae* seeds and preparation of isothiocyanate and amine metabolites, J. Sci. Food Agric. 86 (2006) 1271–1280.
[40] R. Tsao, Q. Yu, I. Friesen, J. Potter, M. Chiba, Factors affecting the dissolution and degradation of oriental mustard-derived sinigrin and allyl isothiocyanate in aqueous media, J. Agric. Food Chem. 48 (2000) 1898–1902.
[41] R. Pecháček, J. Velíšek, H. Hrabcová, Decomposition products of allyl isothiocyanate in aqueous solutions, J. Agric. Food Chem. 45 (1997) 4584–4588.
[42] H. Nong, J.-M. Zhang, D.-Q. Li, M. Wang, X.-P. Sun, Y.J. Zhu, J. Meijer, Q.-H. Wang, Characterization of a novel β-thioglucosidase CpTGG1 in *Carica papaya* and its substrate-dependent and ascorbic acid-independent O-β-glucosidase activity, J. Integr. Plant Biol. 52 (2010) 879–890.
[43] M. Goličnik, On the Lambert *W* function and its utility in biochemical kinetics, Biochem. Eng. J. 63 (2012) 116–123.